Flume tests on the hydraulic/mechanical behavior of the Tangjiashan landslide dam considering the influences of the different debris materials in heterogeneous strata

Xi Xiong

Kanazawa University: Kanazawa Daigaku

Tatsunori Matsumoto

Kanazawa University: Kanazawa Daigaku

Zhenming Shi (✉ 94026@tongji.edu.cn)

Tongji University College of Civil Engineering

Feng Zhang

Nagoya Institute of Technology Architecture Design Civil Engineering and Industrial Management Engineering: Nagoya Kogyo Daigaku Shakai Kogakuka Shakai Kogaku Senko

---

Research Article

Abstract

Landslide dams (LDs) usually form from natural debris materials and exhibit heterogeneous strata along both the depth and run-out directions. In addition, an LD usually has a weaker structure than that of undisturbed ground and is more vulnerable to seepage loading. Considering that the surface layer of naturally packed LD materials is generally in an unsaturated state, it is undoubtedly important to investigate the stability of the unsaturated debris materials in the heterogeneous strata of LDs. In this paper, a systematic flume test program was first conducted, in which the Tangjiashan LD was carefully referenced for model design. Three water level rising rates and two stratal arrangements were considered in the flume tests. Then, soil-water-air coupled finite element analyses were conducted to simulate the flume tests, and all the material parameters of the LD materials were carefully determined based on the results of the element tests. A comparison of the test and calculated results shows the possibility of using the proposed numerical method to estimate the occurrence of dam breaching and the risk of LD failure. Moreover, the hydraulic/mechanical behaviors of the LD materials and the heterogeneous strata of the LD were very important to the stability of the Tangjiashan LD. Finally, from an engineering viewpoint, the possibility of utilizing a naturally formed LD and thus not destroying it when it forms is also discussed, e.g., dam breaching risk can be reduced by excavation of a drainage tunnel, and the dam stability can be carefully estimated based on accurate geological data.

1. Introduction

A landslide dam (LD) usually forms from natural debris materials from landslides, avalanches, debris flows, etc., that are often triggered by earthquakes, rainfall, snowmelt, etc. (Ermini and Casagli, 2003; Peng and Zhang, 2012a). Once an LD is formed, water impoundment will result in a landslide-dammed lake (LD lake). An increase in water level can lead to LD failure within a short time after its formation, which threatens the safety of people and property downstream (Zhu et al., 2003). The failure modes of LDs generally include overtopping, piping and sliding failure (Costa and Schuster, 1988), which are similar to those of artificial soil and rockfill dams. However, unlike artificial dams, LD debris materials have a wide grain size distribution from millimeters to meters, even including gap grading with high erodibility (Ermini and Casagli, 2003). In addition, due to the rapid sliding and packing of the debris materials, the strata of LDs are often only partially destroyed and basically are heterogeneous along both the depth and run-out directions (Chang and Zhang, 2010). Therefore, it is undoubtedly important to investigate the stability of LDs considering the influence of the heterogeneous strata of LDs.

Model testing has become an essential method with which to study the stability of LDs, as in the works by Gregoretti et al. (2010), Awal et al. (2011), Chen et al. (2015), Okeke and Wang (2016), Jiang et al. (2018, 2019) and Dhungana and Wang (2019). In these studies, however, the grain size distribution of the LD material was not considered, and the model LD could only reflect part of a real LD with limitations. Nevertheless, only a few attempts have been made to make the results of LD model tests more credible. Wang et al. (2018) conducted a large-scale model test to identify the premonitory factors of LD failure induced by seepage using material sourced from the Mihata LD. Xiong et al. (2018) selected three typical

LD materials to investigate the failure mechanism of unsaturated LDs under seepage loading. Peng et al. (2019) carried out a series of wave flume tests on the erosion failure modes of LDs, and the typical gradation curve of the Donghekou LD was selected to prepare the dam material. In particular, based on field investigations of an LD in the Xiaoqinling gold mining area, flume tests were conducted with mine waste material, from which particles with diameters >50 mm were removed (Zhu et al., 2019).

In the abovementioned studies, however, all LD models were uniformly prepared, and the presence of heterogeneous strata in LD was ignored. Therefore, in this research, a systematic flume test program was conducted, and a specific LD, named the Tangjiashan LD, was referenced for model design. Particular attention was paid to the influence of the model ground made of different debris materials and heterogeneous strata from the Tangjiashan LD.

Notably, the Tangjiashan LD did not naturally fail, it was partially triggered due to the erosion of overtopping water after digging a spillway to reduce the water level of the LD lake. Therefore, many studies have mainly focused on the breaching process, as in the works by Liu et al. (2009), Chang and Zhang (2010), Fan et al. (2012), Peng and Zhang (2012b) and Shi et al. (2015b). Basically, an LD has a weaker structure than that of the undisturbed rock mass before landsliding and is more vulnerable to seepage loading. Because it is very complicated to estimate the stability of an LD under seepage loading (Xiong et al., 2018), only a few studies have focused on the seepage stability of the Tangjiashan LD. Shi et al. (2018) proposed a coupled computational fluid dynamics and discrete element method (CFD-DEM) model to simulate seepage tests on the material of the Tangjiashan LD, in an attempt to reveal the seepage failure mechanism from macro and micro perspectives. Based on accurate geological data from the Tangjiashan LD, Hu et al. (2012) simulated the seepage flow of the Tangjiashan LD under four water level conditions and discussed its seepage stability. However, the surface layer materials of LDs are usually in an unsaturated state, and their strengths are dependent on the degree of saturation, which has not been properly considered in past studies related to the seepage stability analyses of the Tangjiashan LD.

Therefore, this research aimed to study the stability of an unsaturated LD under seepage loading conditions while considering the influence of different debris materials in the heterogeneous strata of the LD. A systematic flume test program was conducted first, in which the Tangjiashan LD was referenced for model design. The development of the phreatic line in the model LD was carefully measured using sensors, including piezometers, water content sensors and tensiometers. Then, in the corresponding simulation, a saturated/unsaturated soil constitutive model and a deformation-dependent water retention curve (WRC) model (Xiong, 2020) were selected. The parameters of the debris materials of the LD were carefully determined using the results of element tests (Shi et al., 2018; Xiong et al., 2018; Ma et al., 2020), based on which the flume tests on the hydraulic/mechanical behavior of the Tangjiashan LD were simulated with soil-water-air coupled finite element analyses.

2. Geological Background Of The Tangjiashan Landslide Dam

On May 12, 2008, a 8.0 M_s earthquake occurred in Wenchuan County, Sichuan Province, China, and triggered at least 257 LDs (Cui et al., 2009). The Tangjiashan LD was the largest LD located on the Tongkou River 6 km upstream of Beichuan County, as shown in Photograph 1(a). The Tangjiashan LD was 803.4 m in longitudinal length, 611.8 m in maximum transversal width and 82.7-124.4 m in height. The upstream slope of the Tangjiashan LD was 18°-22°, and its average downstream slope was 38° (Liu et al., 2009). The estimated volumes of the accumulated debris mass and LD lake were 2.04×10^7 m^3 and 3.16×10^8 m^3, respectively, posing a great threat to Beichuan County.

According to site investigation results, the Tangjiashan LD maintained a part of the original stratum structure (Fig. 1). It mainly consists of four materials: (1) gravely soil, distributed on the top with a thickness of 5-15 m (Photograph 2); (2) strongly weathered cataclasite, a kind of cohesive granular fault rock, distributed in the middle with a thickness of 10-30 m (Photograph 3); (3) weakly weathered cataclasite, distributed on the bottom with a thickness of 50-67 m (Photograph 4); and (4) silty sand, mainly distributed on the upstream slope of the dam (Photograph 5).

After the formation of the LD, the water level of the Tangjiashan LD lake first rapidly increased and then gradually increased, as shown in Fig. 2. During the rise of the water level, concentrated seepage points with stable flow were observed at elevations of 669 m and 700 m on the downstream slope of the dam. The water from all these seepage points was clear, indicating that piping did not occur in the dam body. Considering the continuous increase in water level, a spillway with a depth of 12 m was constructed across the Tangjiashan LD (Shi et al., 2015b). Dam breaching finally occurred on June 7, 2008 due to overtopping. The majority of the dam mass, especially the weakly weathered cataclasite layer, however, remains stable, as shown in Photograph 1(b).

In brief, three important characteristics of the Tangjiashan LD were observed: (a) the debris materials of the Tangjiashan LD are obviously zoned, which can satisfy the purpose of this research; (b) before breaching, seepage did develop in the dam body, showing the necessity to clarify its influence on the Tangjiashan LD; (c) the debris materials of the Tangjiashan LD were not completely breached. These three characteristics were carefully considered in designing the model LD to investigate the influence of different debris materials in heterogeneous strata on LD stability using flume tests and corresponding numerical simulations.

3. Flume Test

3.1. Ground materials for flume tests

As mentioned before, the debris materials of LDs exhibit a wide range of grain size distributions. The proper selection of debris materials in flume tests is a very important issue. Due to the lack of information about the grain size distribution curves of debris materials in Tangjiashan LD, three typical debris materials of LDs were utilized as the test materials in the flume tests and numerical calculations of this research. Fig. 3 shows the grain size distribution curves of these debris materials. Element tests have

been conducted on these materials, including triaxial tests, water retention tests, and permeameter tests, and satisfactory results have been obtained (Shi et al., 2018; Xiong et al., 2018; Ma et al., 2020).

To assure the operability and repeatability of the flume tests and their corresponding numerical calculations, three different manmade LD debris materials were prepared by mixing different silica sands with grading curves, as shown in Fig. 3. Without losing the general properties of the debris materials, such as permeability and strength, particles greater than 40 mm were removed and not used in the model tests. These three grading curves represent (1) sand, (2) a well-graded mixture and (3) a gap-graded mixture. For simplicity, hereafter, the manmade LD debris materials are called LD materials.

By comparing the hydraulic/mechanical behaviors of the three typical LD materials (Shi et al., 2018; Xiong et al., 2018; Ma et al., 2020) with those of the Tangjiashan LD materials, the sand, well-graded mixture and gap-graded mixture were selected to represent the silty sand, the strongly weathered cataclasite, and the gravely soil of the Tangjiashan LD, respectively. Meanwhile, bricks with high strength and high erosion resistance properties were used to represent the weakly weathered cataclasite in this research.

Permeameter tests on these LD materials under a saturated condition were conducted by Shi et al. (2015b), who found that the permeability of sand, well-graded and gap-graded LD materials in a saturated state were k_{sw}= 8.72×10^{-4}, 3.33×10^{-4} and 1.29×10^{-4} m/s, respectively, with an average void ratio of e_0=0.48.

3.2. Setup of flume tests and LD model

A flume with a rectangular section was utilized in this paper; the flume was 50 m in length, 0.8 m in width, 1.25 m in height and had a 0° slope angle. More details about the flume can be found in Xiong et al. (2018).

The longitudinal section of the Tangjiashan LD along the river, as shown in Fig. 1, was simplified with layered strata, as shown in Fig. 4. The height-to-length ratio of the model LD was small, only 2:9, which is an important characteristic of LDs and distinctly different from the geometry of artificial dams (Costa and Schuster, 1988). Based on the maximum dry density obtained from the compaction tests, the initial dry density of the ground materials in the model LD was determined and is presented in Table 1. The designed compaction degree of the sand and gap-graded mixture on the surface of the dam model was 75%, and the designed compaction degree of the well-graded mixture in the interior was 80%. According to the Froude similarity law, when the geometric scale is 1:300, the time scale is , the velocity scale is , and the density scale is 1 in a 1g gravitational field.

As shown in Fig. 5, the measuring system consists of three piezometers, five water content sensors, five tensiometers, three video cameras, two displacement transducers and three data acquisition instruments, which were used to monitor the deformation and seepage of the model LD. The water content sensors were EC-5 sensors, made by METER Group, Inc. USA, and can measure volumetric water contents from

0% to 100%. The tensiometers were ML-2100AM6 tensiometers, made by Mol, Inc., Japan, and can measure pore pressures from -100 kPa to +100 kPa. To reduce the influence of the tensiometer as an alien component of the model ground on the seepage in the dam body, an L-shaped plastic plate was fixed in the flume, as shown in Fig. 6. Through small holes on the vertical plastic plate, tensiometers can be arranged more reliably.

3.3. Test methodology

To investigate the stability of the LD under seepage loading conditions, four flume tests were conducted considering the different debris materials in heterogeneous strata of the LD. Based on the simplified model LD shown in Fig. 4, the layers of the gap-graded mixture, well-graded mixture and brick had different thicknesses in different cases. As shown in Table 2, the layer thicknesses of the different materials in Case A-1 and Case A-2 are the same as the corresponding layer thicknesses of the Tangjiashan LD after scaling down the observations 300 times. Meanwhile, in Case B-1 and Case B-2, the layer thicknesses of the gap-graded mixture and well-graded mixture were increased to 120 mm to investigate their influence on the development of the phreatic line.

Moreover, the influence of the water level rising rate (WLRR) on the hydraulic/mechanical behavior of the LD was also studied, as shown in Table 2. Considering the control accuracy of the inflow valve, the WLRR in Case A-2 was set to 3 mm/min. The WLRR in Case A-1 was set to three times faster than that in Case A-2. Moreover, the WLRRs in Case A-2 and Case B-1 were the same. Considering the changes in the WLRR of the Tangjiashan LD shown in Fig. 2, the water level in Case B-2 was set to increase at 3 mm/min to 160 mm and then increased at 1 mm/min to the crest of the model LD.

In the tests, the LD materials were first prepared by mixing dry silica sands with different grain sizes to reach the prescribed grain size distribution curves, as shown in Fig. 3. Then, the bricks were stacked in the shape shown in Figure 4, and the surface layer of bricks was mortared with a mixture of water-cement-clay at a mass ratio of 1:2:2 to reduce its permeability. The other parts of the model LD were prepared by compacting every layer to a 40-mm thickness according to the sizes and compaction degrees shown in Fig. 4, Table 1 and Table 2. After that, an initial water level of 50 mm was added on both sides of the model LD, and the measurement system was started. After 1 h, the data from the piezometers were stable, and all the measuring devices were set to zero, which was regarded as the beginning of the test. Next, the water level was raised gradually on the left side of the model LD according to the rate listed in Table 2. Simultaneously, all the measuring devices were started to record the acquired data at regular intervals. Except for Case B-2, the water level upstream was set to increase continually until the model LD failed by overtopping. Considering the situation that the model LD did not fail after overtopping, the inflow valve was closed after the water level reached the crest of the model LD in Case B-2.

3.4. Test results

Since the model LD was under a plane strain state, the sensors, which were set perpendicular to the side of the model LD (e.g., T1 and W1), measured the values of the same point. Consequently, the relation

between the suction and water content of a measuring point can be obtained from the values of the tensiometer and water content sensor at that point. According to the test results, the model LD failed by overtopping in Case A-1, Case A-2 and Case B-1, while the failure mode of the model LD in Case B-2 was sliding failure. Moreover, the development processes of the seepage in the dams were different among the different cases. Unfortunately, some sensor data were missing due to technical issues. The available results of each case are introduced in detail as follows.

The results of Case A-1 are shown in Fig. 7 and Photograph 6. As shown in Fig. 7(b), with the increase in water level, the suction at all measuring points remained constant at first. Then, the suction at T1 decreased significantly at T= 29 min, while the suction at other measuring points began to decrease at almost the same time (T=32 min). Meanwhile, it was also observed in Fig. 7(c) that the increase in water content at W1 was earlier than that at other measuring points. The reason for this phenomenon is that the model LD began to breach at T=31 min due to overtopping; the failure process is shown in Photograph 6. The soil at T1-W1 was saturated by the seepage flow from the upstream before overtopping, while the soils at other measuring points were saturated by water from the crest after overtopping. Since the infiltration path was significantly shortened, the soils at T2-W2, T3-W3, T4-W4 and T5-W5 almost became saturated at the same time. Thus, with a WLRR of 10 mm/min, the phreatic line developed to T1-W1 before overtopping, and the whole dam saturated quickly after overtopping.

The results of Case A-2 are shown in Fig. 8 and Photograph 7. As shown in Figs. 8(a) and (e), with the increase in the water level, the excess pore water pressure (EPWP) at P1 and P2 increased gradually, and their increments were approximately the same. This phenomenon indicates that sand can be easily saturated because of its high permeability, and the phreatic line in the upstream slope of the model LD was approximately horizontal. In addition, Figs. 8(b) and (c) show that the suction at T1-W1 started to decrease at T=118 min and that the phreatic line developed to T1-W1 at T=130 min. With the saturation of the upper layers in the dam, the vertical displacement at DS1 increased gradually, as shown in Fig. 8(f). Since the vertical displacement at DS2 was mainly contributed by dam breaching, the vertical displacement at DS2 was greater than that at DS1 at the end of the test. Dam breaching was triggered by overtopping at T=151 min, and the failure process is shown in Photograph 7.

For Case B-1, the WLRR was similar to that of Case A-2, as shown in Fig. 9(a). However, compared with that in Case A-2, the model LD in Case B-1 had a thinner brick layer and thicker soil layers, indicating that the soil of the well-graded mixture layer exhibited different initial states. Compared to the other layers, the well-graded mixture layer was closer to the initial water level, so the soil at T3-W3 and T5-W5 had lower initial suctions and higher initial water contents, as shown in Figs. 9(b) and (c). In addition, with the increase in water level, the suction at both T3-W3 and T5-W5 decreased gradually, and the water content increased gradually, which means that the phreatic line was approaching these two measuring points. As a result, the phreatic line in Case B-1 was able to develop downstream further than those in the other cases. Fig. 9(f) also shows that the vertical displacement of DS1 at the end of Case B-1 was greater than that of Case A-2. Therefore, the increase in the thickness of the soil layers might have led to greater vertical displacement at the dam crest during the increase in the water level. The decrease in the height of

the dam crest could lead to earlier overtopping failure. In other words, the increase in the thickness of soil layers reduced the stability of the LD, a comprehensive result. The failure process of the model LD in Case B-1 is shown in Photograph 8.

In Case B-2, unlike in other cases, the water level decreased gradually to 337 mm after reaching the dam crest, as shown in Fig. 10(a). Fig. 10(b) shows that the suction at T3 and T5 decreased during the whole test, and the suction at T2 and T4 also began to decrease after T= 210 min. Moreover, the suction at all the measuring points reached 0 kPa at the end of the test. Hence, although the permeability of the gap-graded mixture was the lowest, the gap-graded mixture layer could also become saturated under seepage conditions. Interestingly, as shown in Fig. 10(d), although the s-q relation curves of the gap-graded mixture and the well-graded mixture are different, they are similar to the water retention curves obtained from water retention tests on corresponding materials (Ma et al., 2020). Finally, Fig. 10(e) shows that the vertical displacement at DS2 suddenly decreased at T= 1024 min, indicating the occurrence of a landslide. The landslide mass was composed of only the gap-graded mixture, as shown in Photograph 9.

According to the measurement data and the observed phenomenon, the development of the phreatic line in the model LD was estimated, as shown in Fig. 11. The flume test results indicate that the stability of the LD under seepage loading is significantly influenced by the different debris materials in its heterogeneous strata. To obtain more detailed information, numerical simulations of the flume tests were conducted utilizing a suitable saturated/unsaturated constitutive model. Notably, according to the s-q relation for the model LD, as shown in Fig. 9(d) and 10(d), the water content could increase under constant suction conditions, which means that a deformation-dependent WRC model is necessary for accurate numerical simulation.

4. Numerical Simulation Of The Flume Tests

4.1. Saturated/unsaturated constitutive model and WRC model

The results of triaxial tests on three typical LD materials (Ma et al., 2020) indicate that the LD materials have a highly developed soil structure, as shown in Fig. 13. To accurately describe the behavior of LD materials, an unsaturated soil constitutive model (Xiong, 2020) was selected. To consider the structure of the soils formed in the natural deposit process, Xiong (2020) incorporated the concept of superloading (Asaoka et al., 2000) into a present constitutive model proposed by Zhang and Ikariya (2011), which utilizes skeleton stress and degree of saturation as independent variables. There are some studies on the application of the constitutive model (Zhang and Ikariya, 2011) in calculating the stabilities of an unsaturated slope and LD, and reasonable results have been observed—e.g., Xiong et al. (2014) and Xiong et al. (2018).

In addition, to properly consider the influence of deformation on the degree of saturation, a WRC model proposed by Xiong (2020) was also utilized. Based on the experimental evidence, in this model, it is assumed that if subjected to only volumetric deformation, the shape of the intrinsic WRC at any void ratio

does not change, but the curve shifts parallel to the S_r axis in S_r-s space. Coupled with the constitutive model, the WRC model has been used to describe the hydraulic/mechanical behavior of completely decomposed granite, and satisfactory accuracy has been observed (Xiong, 2020). Thus, it is reasonable to select this WRC model to simulate the development of the phreatic line in the model LD.

4.2. Parameter determination

In this research, to ensure the accuracy of the boundary value problem calculations, all the material parameters involved in the constitutive model of the saturated/unsaturated soil are determined via the element tests. The parameters involved in constructing the WRCs for the three LD materials were determined from the water retention tests (Xiong, 2020; Ma et al., 2020), and their values are listed in Table 3. The material parameters were essentially determined by the saturated triaxial test results (Ma et al., 2020) considering the available physical quantities obtained by the water retention tests. The calibrated material parameters of the three LD materials are listed in Table 4.

Fig. 12 shows a comparison of the tested and simulated results of the water retention tests with the parameter values listed in Tables 3 and 4. Generally, the calculated results agree well with the experimental data. Thus, the WRC model coupled with the unsaturated soil constitutive model (Xiong, 2020) can describe both the skeleton curves and scanning curves of LD materials with satisfactory accuracy.

Fig. 13 shows the element simulation of triaxial compression tests on saturated LD materials, and the values of the corresponding parameters are listed in Tables 3 and 4. Good agreement between the calculated and test results is observed, although some discrepancies exist. Throughout the shearing stage, the stress difference of the calculated and test results of the sand increases, while the stress differences of the well-graded mixture and gap-graded mixture first increased and then gradually decrease. Moreover, the calculated EPWP is able to capture the overall trend of the tested EPWP. Therefore, numerical method used in this paper is able to properly describe the strain-stress-dilatancy relation of LD material in triaxial tests.

In the calculations, the saturated permeability of the LD materials was set according to the results of the permeameter tests conducted by Shi et al. (2015b). The unsaturated permeability of the LD materials was set by the formula of van Genuchten (1980).

Considering the high strength of the brick, its stress-strain relation was described by an elastic model. The material parameters of the brick in the numerical calculations were set as follows: Young's modulus of 30 MPa, Poisson's ratio of 0.25, specific gravity of 2.8 and permeability of 8.54×10^{-6} m/s.

4.3. Numerical model and initial conditions

The flume tests of the model LD were simulated with the soil-water-air coupled FEM program SOFT (Xiong et al., 2014), using the finite element-finite difference (FE-FD) scheme for soil-water-air three-phase

coupling problems. There are five cases in the numerical calculation, as shown in Table 5. In Case A-1, Case A-2, Case B-1 and Case B-2, the values of the soil parameters were the same as those listed in Tables 3 and 4. To investigate the influence of the soil deformation on the development of the phreatic line, numerical calculation Case A-0 was conducted, which had the same WLRR and strata as Case A-2 but different soil parameters. In Case A-0, the parameter c_e of the WRC model that controls the influence of deformation on the degree of saturation was set to 0.0 in all the LD materials.

The finite element mesh used in the simulation was built according to Fig. 4, of which the size is the same as that of the model LD under plane strain conditions, as shown in Fig. 14. The finite element mesh is composed of 1351 nodes and 1255 4-node isoparametric elements.

Fig. 15 shows the boundary conditions in the settings of the numerical model. Fig. 15(a) shows that drainage and vented boundary conditions are exactly the same as those for the flume tests. For the displacement boundary condition, as shown in Fig. 15(b), the bottom surface is fixed in the x and y directions, and the other surfaces are free in both directions.

In addition to the boundary conditions, the setting of the initial conditions is also crucial in numerical simulation and will greatly affect the accuracy of the calculation. Since the model LD was prepared via the layered compaction method, the materials were heavily compacted at the initial condition. Mean effective stress of 12 kPa was added to the whole area to consider the compaction effect by comparing the simulated and test results. Fig. 16 shows the initial mean effective stress field of the calculations.

For the suction and degree of saturation, the initial valves were essentially determined using the data measured during the flume tests and the WRC curves of the LD materials (Xiong et al., 2018; Ma et al., 2020), as shown in Table 5. Notably, the initial suction in the numerical calculations, 4 kPa or 6 kPa, is lower than the data measured during the flume tests. Xiong et al. (2018) and Ma et al. (2020) conducted water retention tests on LD materials with maximum grain sizes of 40 mm and 2 mm, respectively. The test results show that LD materials with a maximum grain size of 40 mm have a much lower suction at the residual degree of saturation state. Hence, the conclusion can be drawn that particles with grain sizes greater than 2 mm also influence the water retention properties of LD materials. Considering that the length of a tensiometer probe is only 15 mm, the suction measured during the flume tests could be the local suction of small particles in the LD materials. Therefore, it is reasonable to set the initial suction in the numerical calculations as shown in Table 5.

A water head of 50 mm was loaded on the upstream slope of the model LD in the initial stage of the numerical simulations. After 1 h, the physical quantities at this moment were regarded as the initial state of the model LD (T=0 min). Subsequently, a prescribed increment of water head is applied to simulate the variation in water level. The WLRR of Case A-0 was set to be the same as that of Case A-2. Except for Case B-2, for all the other cases, after the water head peaked, a 420 mm high water head was quickly applied to the crest and the downstream slope of the model LD to simulate the overtopping process. At this time, in Case B-2, the upstream water level was unloaded to 337 mm over the following 600 min.

4.4. Flume test simulations

To demonstrate the performance of the numerical method used in this research, the calculation results for Case A-0 and Case A-2 are first compared with the experimental results. Fig. 17 and Fig. 18 show the distributions of the degree of saturation at different times in Case A-0 and Case A-2, respectively. When considering the influence of the deformation on the WRC, the phreatic line can clearly develop further downstream. Compared with the tested results shown in Fig. 11(b), the calculation result for Case A-2 coincides better with the tested development of the phreatic line. Therefore, the numerical method used in this paper is proved to have an accuracy that can adequately describe the development of phreatic lines in flume tests.

Fig. 19 shows the test and simulated results for the mechanical quantities of Case A-2. Fig. 19(a) shows that the rising rates of the EPWP at P1 and P2 are approximately the same, and the maximum EPWP at P2 is greater than that at P1; these results are in good agreement with the test results. As shown in Fig. 19(b), the magnitude and the trend of the vertical displacement obtained from the test and the simulation are essentially the same. Although the breaching process of the LD cannot be completely simulated using the FEM, the simulated vertical displacement at DS2 decreased suddenly at T=149 min, which can indicate the occurrence of dam breaching. Moreover, once the overtopping breaching of an LD occurs, the entire breaching process will continue and cannot stop (Yang et al., 2015). The time of the occurrence of dam breaching is called the longevity of the LD in this research. Therefore, the numerical method proposed in this research can be utilized to estimate the occurrence of dam breaching and the longevity of the LD.

Fig. 20 shows the distribution of the degree of saturation at different times in Case A-1. Compared with Case A-2, although the WLRR tripled in Case A-1, the phreatic lines at the same water level almost coincided. In addition, the maximum vertical displacement at DS1 in Case A-1 was 11.75 mm and slightly smaller than that in Case A-2, as shown in Fig. 19(b) and 21(b). The longevity of the model LD in Case A-1 was 34 min, which was one-third shorter than that in Case A-2. Therefore, although the WLRR has little influence on the development of the phreatic line in the model LD, its increase can reduce the stability of the model LD.

For Case B-1, the phreatic line developed much further downstream, as shown in Fig. 22. Since the model LD in Case B-1 had thicker soil layers and a lower initial suction than those in Cases A-1 and A-2, the LD materials were more easily saturated by seepage. Fig. 23(a) shows that the EPWP at P3 increased to be greater than that at P2 in both the tested and simulated results. In addition, according to the simulated vertical displacement at DS2 shown in Fig. 23(b), the longevity of the model LD in Case B-1 was 156 min, which was longer than that of the model LD with the same WLRR in Case A-2. The reason for this phenomenon is considered that after overtopping, it took more time to completely saturate a model LD with thicker soil layers.

For Case B-2, the phreatic line developed to the downstream slope surface of the model LD, and the well-graded mixture layer was totally saturated at the end of the test, as shown in Fig. 24. Fig. 25 shows good

agreement between the calculated and test results in terms of the changes in EPWP and vertical displacement. Although it is difficult to estimate the occurrence of a landslide by the simulated vertical displacement at DS2, the displacement vectors of the downstream slope in Case B-2 are much greater than those in other cases, as shown in Fig. 26, which can also be used as a basis for determining the occurrence of a landslide. Moreover, Fig. 26(d) shows that the displacement is mainly concentrated in the gap-graded mixture layer. According to the triaxial test results of the LD materials (Ma et al., 2020), the strength of the gap-graded mixture is the lowest, and it is most intolerable to the seepage loading, which can explain why the landslide mass was composed only of the gap-graded mixture, as shown in Photograph 9.

A comparison between the test and the calculated results of all the test cases shows that based on a rational constitutive model and a deformation-dependent WRC model, the numerical method proposed in this study offers satisfactory accuracy for describing the stability of an LD under seepage loading conditions. Moreover, the hydraulic/mechanical behaviors of the LD materials and the heterogeneous strata of the LD play an important role in its stability. The height of the dam crest decreased with increasing water level due to the saturation of the LD materials. Hence, increasing the thickness of the soil layers can reduce the stability of an LD. In addition, owing to the low strength of the gap-graded mixture, sliding failure of the Tangjiashan LD could occur in the gap-graded mixture layer when the LD lake had a high water level. However, due to the small height-to-length ratio of the Tangjiashan LD, the phreatic line in the dam body is difficult to develop on the surface of the downstream slope before overtopping breaching. As a result, regardless of whether the spillway is constructed, with a continuously increasing upstream water level, even though its rising rate is small, Tangjiashan LD would fail by overtopping after formation.

Therefore, the construction of a spillway on the Tangjiashan LD only caused the earlier occurrence of overtopping and did not increase the stability of the dam body. Considering the different debris materials in the heterogeneous strata of the Tangjiashan LD, it is essential to increase the stability of the dam body by controlling the water level of the LD lake. For example, excavation of a drainage tunnel through the Hongshiyan LD successfully reduced the dam breaching risk (Shi et al., 2017), and this LD was then rebuilt into a large-integrated water conservancy complex (Zhang et al., 2020). If engineering measures would have been taken to control the water level below the gap-graded mixture layer, the Tangjiashan LD could have maintained stability, and the water resources of the LD lake could have been reasonably controlled and sufficiently utilized.

5. Conclusions

In this paper, taking the Tangjiashan LD as a reference example, a systematic flume test program was conducted with three typical LD materials subjected to rising water levels. Particular attention was paid to the influence of different debris materials in the heterogeneous strata on the LD stability. Meanwhile, soil-water-air coupled finite element analyses, based on a constitutive model for saturated/unsaturated soils

and a finite deformation-dependent WRC model (Xiong, 2020), were conducted to simulate the corresponding flume tests as boundary value problems. The following conclusions were obtained.

1. From the geological and hydrological information of the Tangjiashan LD, three important characteristics were summarized, suggesting that proper selection of the debris materials for the model LD and careful zoning of the strata are necessary for clarifying the hydraulic/mechanical behaviors of LDs subjected to rising water levels.

2. The flume tests of the model LDs showed that the stability of an LD under seepage loading conditions is significantly influenced by the different debris materials in its heterogeneous strata. The model LDs failed by overtopping in Case A-1, Case A-2 and Case B-1, while the failure mode of the model LD in Case B-2 was sliding failure, and the landslide mass was limited to the layer of gap-graded mixture. From the measured data and observed phenomena, the development of the phreatic line in the model LD was successfully identified, e.g., it developed much further downstream in Case B-1 and Case B-2 than in the other cases.

3. A comparison of the results from the flume tests and the corresponding numerical calculations indicates that the proposed numerical method can describe the behavior of an LD subjected to a rising water level with satisfactory accuracy. It is clarified for the first time that the calculations that adopt the deformation-dependent WRC model can describe the observed phreatic line much better than those that do not adopt the deformation-dependent WRC model, showing the possibility of using the proposed numerical method to estimate the occurrence of dam breaching and the risk of LD failure.

4. As the water level increased, settlement of the dam crest occurred due to the saturation of the LD materials. Hence, the thicker the soil layer is, the lower the stability of the LD. In addition, owing to the low strength of the gap-graded mixture, sliding failure of the Tangjiashan LD might occur in the gap-graded mixture layer under seepage conditions.

5. Due to the small height-to-length ratio of the Tangjiashan LD, it is difficult for the phreatic line in the dam body to reach the surface of the downstream slope before overtopping breaching. As a result, with a continuous increase in the upstream water level, even though its increasing rate is small, the Tangjiashan LD will fail by overtopping without any treatment. The construction of a spillway on the Tangjiashan LD only caused the overtopping breaching to occur earlier but did not increase the stability of the dam body. Therefore, if it is possible to construct a diversion tunnel to avoid overtopping of LD, it might a wiser way not to destroy an LD whenever it is formed. From an engineering viewpoint, it is possible to utilize a naturally formed LD instead of destroying it. For example, the dam breaching risk can be reduced by excavation of a diversion tunnel on the condition that the dam stability is carefully estimated based on not only accurate hydraulic and geological data but also construction conditions.

Declarations

References

Asaoka A, Nakano M, Noda T (2000) Superloading yield surface concept for highly structured soil behavior. Soils Found 40(2): 99-110. https://doi.org/10.3208/sandf.40.2_99

Awal R, Nakagawa H, Kawaike K, Baba Y, Zhang H (2011) Experimental study on piping failure of natural dam. Journal of Japan Society of Civil Engineers, Ser. B1 (Hydraulic Engineering) 67(4): I_157-I_162. https://doi.org/10.2208/jscejhe.67.I_157

Chang DS, Zhang LM (2010): Simulation of the erosion process of landslide dams due to overtopping considering variations in soil erodibility along depth. Nat Hazards Earth Syst Sci: 10(4): 933-946. https://doi.org/10.5194/nhess-10-933-2010

Chen S, Lin T, Chen C (2015) Modeling of natural dam failure modes and downstream riverbed morphological changes with different dam materials in a flume test. Eng Geol 188: 148-158. https://doi.org/10.1016/j.enggeo.2015.01.016

Costa JE, Schuster RL (1988) The formation and failure of natural dams. Geol Soc Am Bull 100(7): 1054-1068. https://doi.org/10.1130/0016-7606(1988)100<1054:TFAFON>2.3.CO;2

Cui P, Zhu YY, Han YS, Chen XQ, Zhuang JQ (2009) The 12 May Wenchuan earthquake-induced landslide lakes: distribution and preliminary risk evaluation. Landslides 6(3): 209-223. https://doi.org/10.1007/s10346-009-0160-9

Dhungana P, Wang F (2019) The relationship among the premonitory factors of landslide dam failure caused by seepage: an experimental study. Geoenvironment Disasters 6(1): 17. https://doi.org/10.1186/s40677-019-0135-7

Ermini L, Casagli N (2003) Prediction of the behaviour of landslide dams using a geomorphological dimensionless index. Earth Surf Process Landf 28(1): 31-47. https://doi.org/10.1002/esp.424

Fan X, Tang CX, Van Westen CJ, Alkema D (2012) Simulating dam-breach flood scenarios of the Tangjiashan landslide dam induced by the Wenchuan Earthquake. Nat Hazards Earth Syst Sci 12(10): 3031. https://doi.org/10.5194/nhess-12-3031-2012

Gregoretti C, Maltauro A, Lanzoni S (2010): Laboratory experiments on the failure of coarse homogeneous sediment natural dams on a sloping bed. J Hydraul Eng-ASCE 136(11): 868-879. https://doi.org/10.1061/(ASCE)HY.1943-7900.0000259

Hu X, Luo G, Wang J, Liu J, Hu H (2010) Seepage stability analysis and dam-breaking mode of Tangjiashan barrier dam. Chin J Rock Mech Eng 29(7): 1409-1417 (in Chinese).

Jiang X, Huang J, Wei Y, Niu Z, Chen F, Zou Z, Zhu Z (2018) The influence of materials on the breaching process of natural dams. Landslides 15(2): 243-255. https://doi.org/10.1007/s10346-017-0877-9

Jiang X, Wei Y, Wu L, Hu K, Zhu Z, Zou Z, Xiao W (2019) Laboratory experiments on failure characteristics of non-cohesive sediment natural dam in progressive failure mode. Environ. Earth Sci 78(17): 538. https://doi.org/10.1007/s12665-019-8544-1

Liu N, Zhang J, Lin W, Cheng W, Chen Z (2009): Draining Tangjiashan Barrier Lake after Wenchuan Earthquake and the flood propagation after the dam break. Sci China, Ser E: Technol Sci 52(4): 801-809. https://doi.org/10.1007/s11431-009-0118-0

Ma J, Xiong X, Yang J, Mikami R, Shi Z, Zhang F (2020) Element tests on hydraulic-mechanical behavior of saturated/unsaturated landslide dam materials. Jpn Geotech Soc Spec Pac 8(9): 360-365. https://doi.org/10.3208/jgssp.v08.j30

Okeke ACU, Wang F (2016) Hydromechanical constraints on piping failure of landslide dams: an experimental investigation. Geoenviron Disasters 3(1): 4. https://doi.org/10.1186/s40677-016-0038-9

Peng M, Jiang QL, Zhang QZ, Hong Y, Jiang MZ, Shi ZM, Zhang LM (2019) Stability analysis of landslide dams under surge action based on large-scale flume experiments. Eng Geol 259: 105191. https://doi.org/10.1016/j.enggeo.2019.105191

Peng M, Zhang LM (2012a) Breaching parameters of landslide dams. Landslides 9(1): 13-31. https://doi.org/10.1007/s10346-011-0271-y

Peng M, Zhang LM (2012b) Analysis of human risks due to dam break floods-part 2: application to Tangjiashan landslide dam failure. Nat Hazards 64(2): 1899-1923. https://doi.org/10.1007/s11069-012-0336-9

Shi, Z.M., Guan, S.G., Peng, M., Xiong, X., 2015a. Research on the influence of material permeability to landslide dam seepage stability. 10th Asian Regional Conference of IAGE, pp. 1-7.

Shi ZM, Guan SG, Peng M, Zhang LM, Zhu Y, Cai QP (2015b) Cascading breaching of the Tangjiashan landslide dam and two smaller downstream landslide dams. Eng Geol 193: 445-458. https://doi.org/10.1016/j.enggeo.2015.05.021

Shi ZM, Xiong X, Peng M, Zhang LM, Xiong YF, Chen HX, Zhu Y (2017) Risk assessment and mitigation for the Hongshiyan landslide dam triggered by the 2014 Ludian earthquake in Yunnan, China. Landslides, 14(1): 269-285. https://doi.org/10.1007/s10346-016-0699-1

Shi ZM, Zheng HC, Yu SB, Peng M, Jiang T (2018) Application of CFD-DEM to investigate seepage characteristics of landslide dam materials. Comput Geotech 101: 23-33. https://doi.org/10.1016/j.compgeo.2018.04.020

Van Genuchten MT (1980) A closed-form equation for predicting the hydraulic conductivity of unsaturated soils. Soil Sci Soc Am J 44(5): 892-898. https://doi.org/10.2136/sssaj1980.03615995004400050002x

Wang F, Dai Z, Okeke CAU, Mitani Y, Yang H (2018) Experimental study to identify premonitory factors of landslide dam failures. Eng Geol 232: 123-134. https://doi.org/10.1016/j.enggeo.2017.11.020

Xiong YL, Bao XH, Ye B, Zhang F (2014) Soil-water-air fully coupling finite element analysis of slope failure in unsaturated ground. Soils Found 54(3): 377-395. https://doi.org/10.1016/j.sandf.2014.04.007

Xiong X, Shi ZM, Guan SG, Zhang F (2018) Failure mechanism of unsaturated landslide dam under seepage loading-Model tests and corresponding numerical simulations. Soils Found 58(5): 1133-1152. https://doi.org/10.1016/j.sandf.2018.05.012

Xiong X (2020) Modeling of hydro-mechanical behavior of unsaturated soils considering finite deformation and its application to unsaturated landslide dam stability. Ph.D. dissertation, Nagoya Institute of Technology, Japan.

Yang Y, Cao SY, Yang KJ, Li WP (2015) Experimental study of breach process of landslide dams by overtopping and its initiation mechanisms. J Hydrodyn Ser. B 27(6): 872-883. https://doi.org/10.1016/S1001-6058(15)60550-9

Zhang Z, Cheng K, Yang Z, Peng F (2020) Key Technology in the Remediation Project of Hongshiyan Landslide-Dammed Lake on Niulan River Caused by "8·03" Earthquake in Ludian, Yunnan. In The International Conference on Embankment Dams, pp. 75-95.

Zhang, F., Ikariya, T., 2011. A new model for unsaturated soil using skeleton stress and degree of saturation as state variables. Soils Found 51(1): 67-81. https://doi.org/10.3208/sandf.51.67

Zhicheng water gauging station (2008) Latest situation of Tangjiashan landslide lake: water level of Zhicheng gauging water level station is 738.85m. http://www.gov.cn/. Accessed 29 April 2020 (in Chinese).

Zhu PY, Wang CH, Wang YC (2003) Large-scale landslide-debris avalanche in Tibet, China, (2) formation of an exceptionally serious outburst flood from a landslide dam in Tibet. Landslide News 14(15): 23-25.

Zhu X, Peng J, Jiang C, Guo W (2019) A preliminary study of the failure modes and process of landslide dams due to upstream flow. Water 11(6): 1115. https://doi.org/10.3390/w11061115

Tables

Table 1 Physical properties of the LD materials used in the flume tests

LD Materials	Specific gravity G_S	Maximum dry density ρ_{dmax} (g/cm^3)	Designed compaction degree D_C (%)	Initial dry density ρ_d (cm^3)
Sand	2.65	2.06	75	1.55
Gap-graded mixture	2.65	2.12	75	1.59
Well-graded mixture	2.65	2.39	80	1.91

Table 2 Test cases of the flume tests

Case	Thickness of layer with gap-graded mixture (mm)	Thickness of layer with well-graded mixture (mm)	Thickness of layer with brick (mm)	Design WLRR (mm/min)
Case A-1	80	80	240	10
Case A-2	80	80	240	3
Case B-1	120	120	160	3
Case B-2	120	120	160	3→1

Table 3 Parameters of the WRC for the LD materials

Materials of LD	Sand	Well-graded	Gap-graded
Degrees of saturation at which suction is zero	0.68	1.00	1.00
Residual degrees of saturation	0.19	0.089	0.14
Parameter corresponding to drying AEV (kPa) S_d	0.90	1.00	13.00
Parameter corresponding to wetting AEV (kPa) S_w	0.20	0.50	1.00
Influence of finite deformation on the degree of saturation c_e	0.2	0.3	0.8
Parameter of shape function c_1	0.65	0.115	0.115
Parameter of shape function c_2	1.4	0.225	0.122
Scanning curve parameter I_d (kPa)	2.5	3.1	3.2
Scanning curve parameter I_0 (kPa)	2.7	2.8	3.7

Table 4 Material parameters of the LD materials involved in the constitutive model

Materials of LD	Sand	Well-graded	Gap-graded
Compression index l	0.089	0.13	0.099
Swelling index k	0.005	0.015	0.0050
Critical state parameter R_{cs}	5.23	4.33	2.55
Void ratio N (p_0 =12 kPa on $N.C.L.$)	0.74	0.44	0.71
Poisson's ratio ν	0.30	0.30	0.2
Parameter of overconsolidation a	5.0	10.	5.0
Parameter of suction b	0.50	3.0	5.0
Parameter of overconsolidation β	5.0	3.0	3.0
Parameter of structure $m*$	0.3	0.45	1.1
Void ratio N_r (p_0 =12 kPa on $N.C.L.S.$)	0.70	0.39	1.24

Table 5 Miscellaneous conditions of the numerical simulations

Case	Consideration of finite deformation in WRC	Sand		Well-graded mixture		Gap-graded mixture	
		s_0 (kPa)	S_{r0}	s_0 (kPa)	S_{r0}	s_0 (kPa)	S_{r0}
Case A-0	No	2	0.25	6	0.30	6	0.60
Case A-1	Yes	2	0.25	6	0.30	6	0.60
Case A-2		2	0.25	6	0.30	6	0.60
Case B-1		2	0.25	4	0.30	4	0.60
Case B-2		2	0.25	4	0.30	4	0.60

Figures
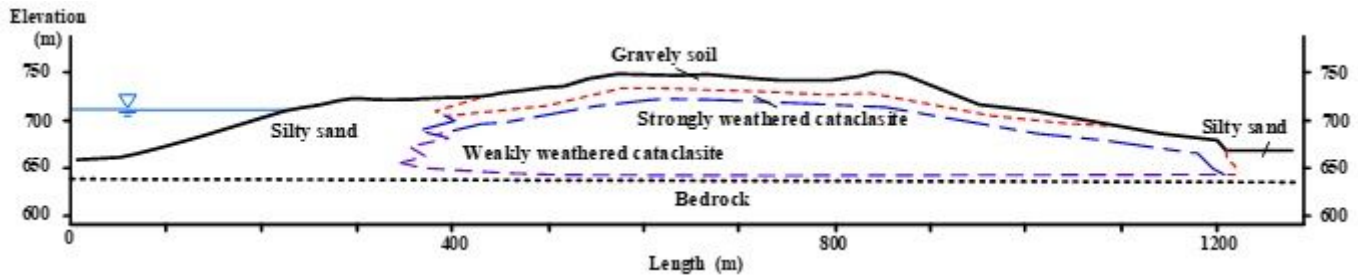
Figure 1

Longitudinal section of the Tangjiashan LD along the river
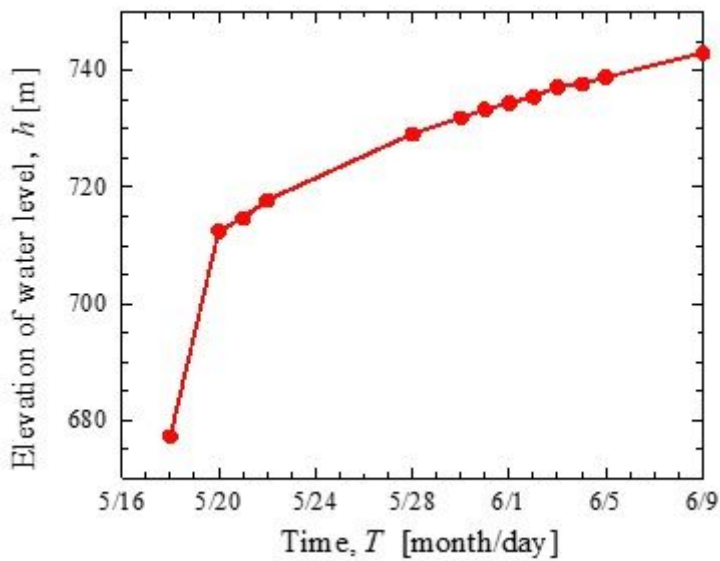
Figure 2

Elevation of water level at the Tangjiashan LD lake (data from Zhicheng water gauging station (2008), close to the upstream of the Tangjiashan LD)
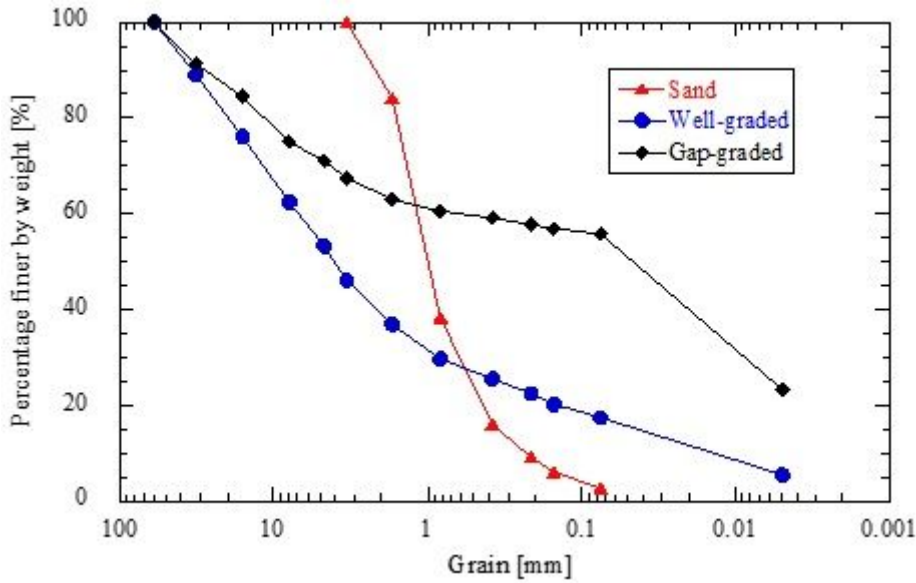
Figure 3

Grain size distribution curves of the LD materials used in the flume tests
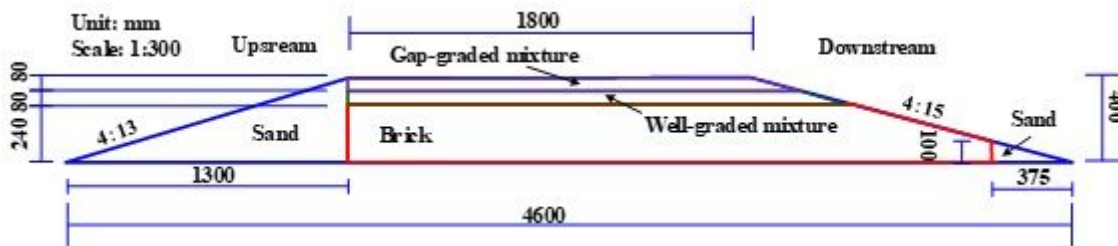
Figure 4

Longitudinal section of the model Tangjiashan LD
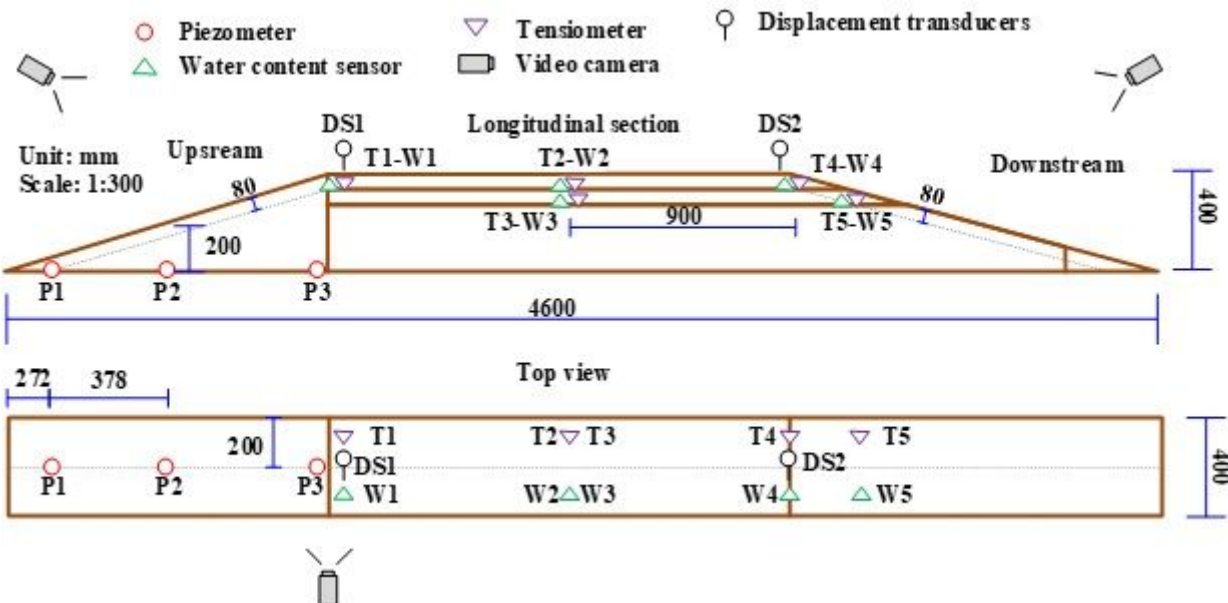
Figure 5

Arrangement of measurement devices set in the model LD
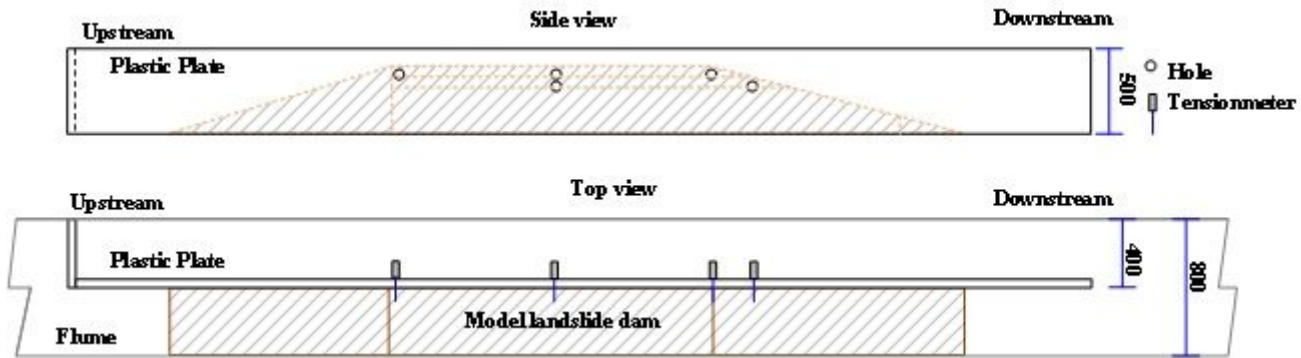
Figure 6

Side and top views of the tensiometers set in the model ground whose thickness is half the width of the flume and supported with a side plastic plate

(a)

(b)

(c)

(d)
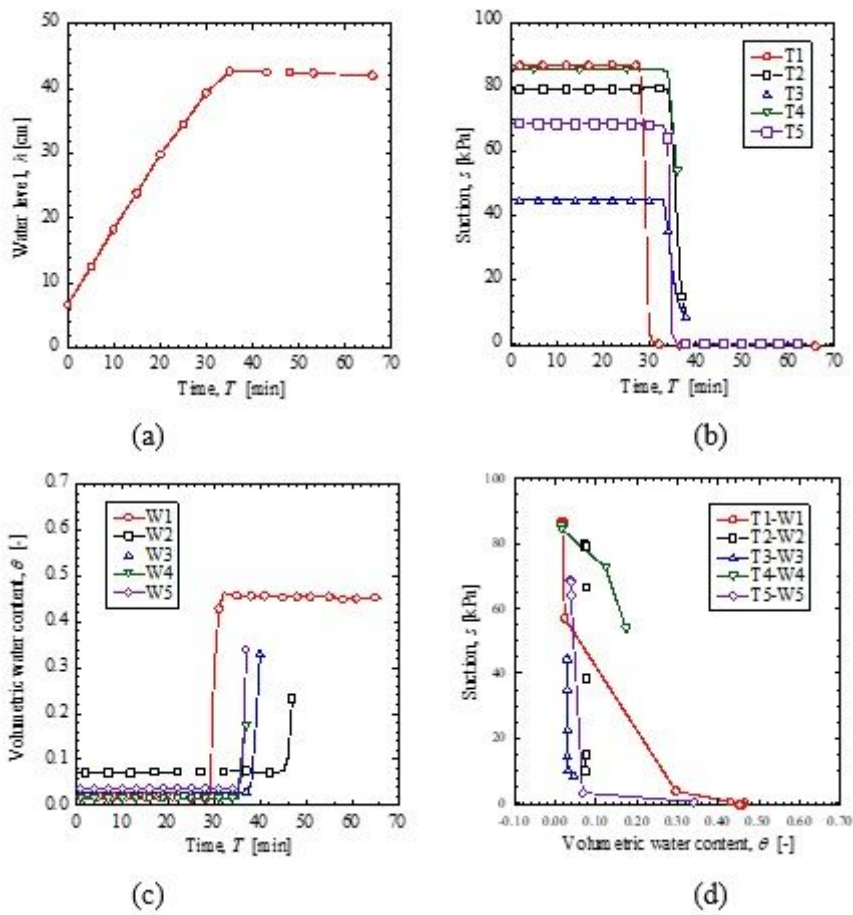
Figure 7

Time histories of the measured results of the Case A-1 flume test
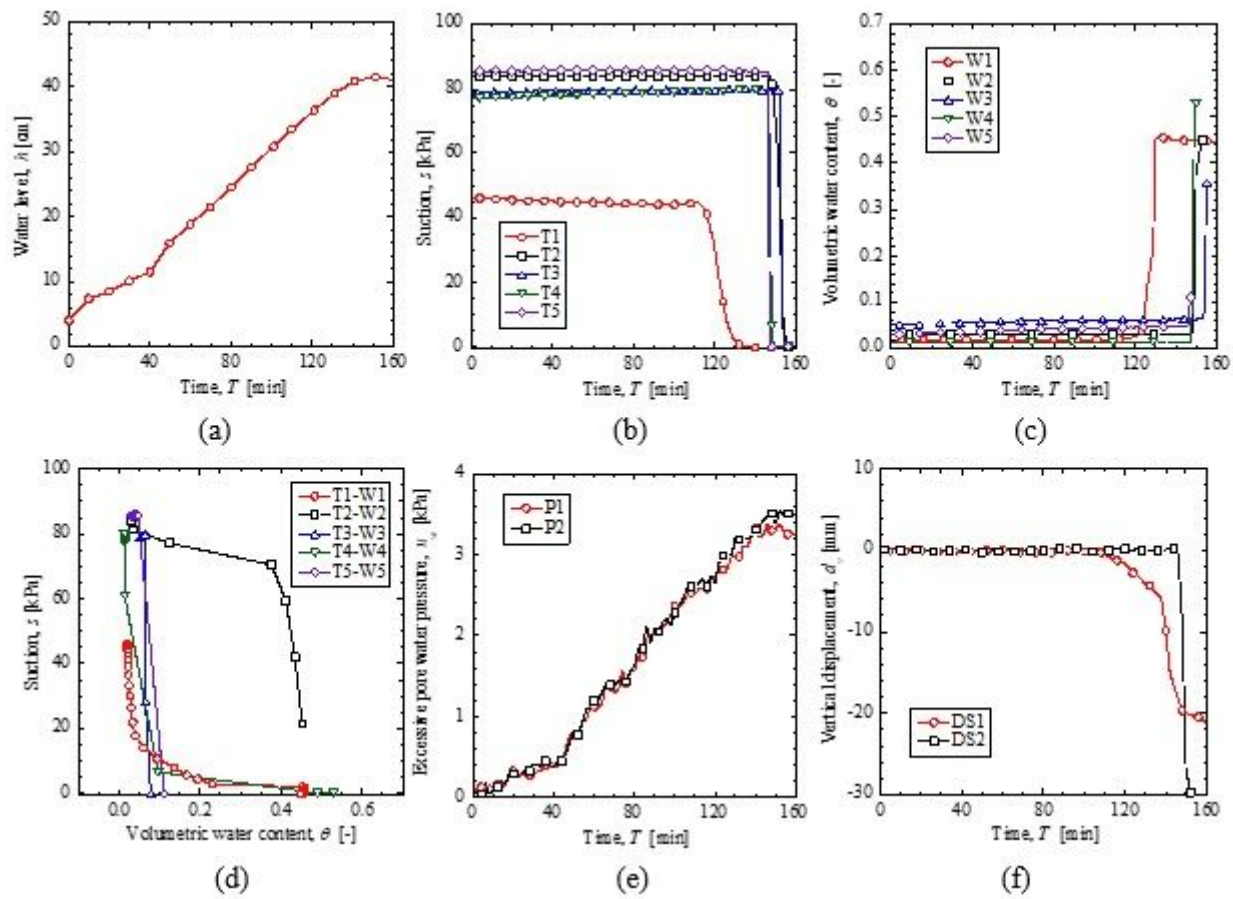
Figure 8

Time histories of the measured mechanical and physical quantities in the Case A-2 flume test
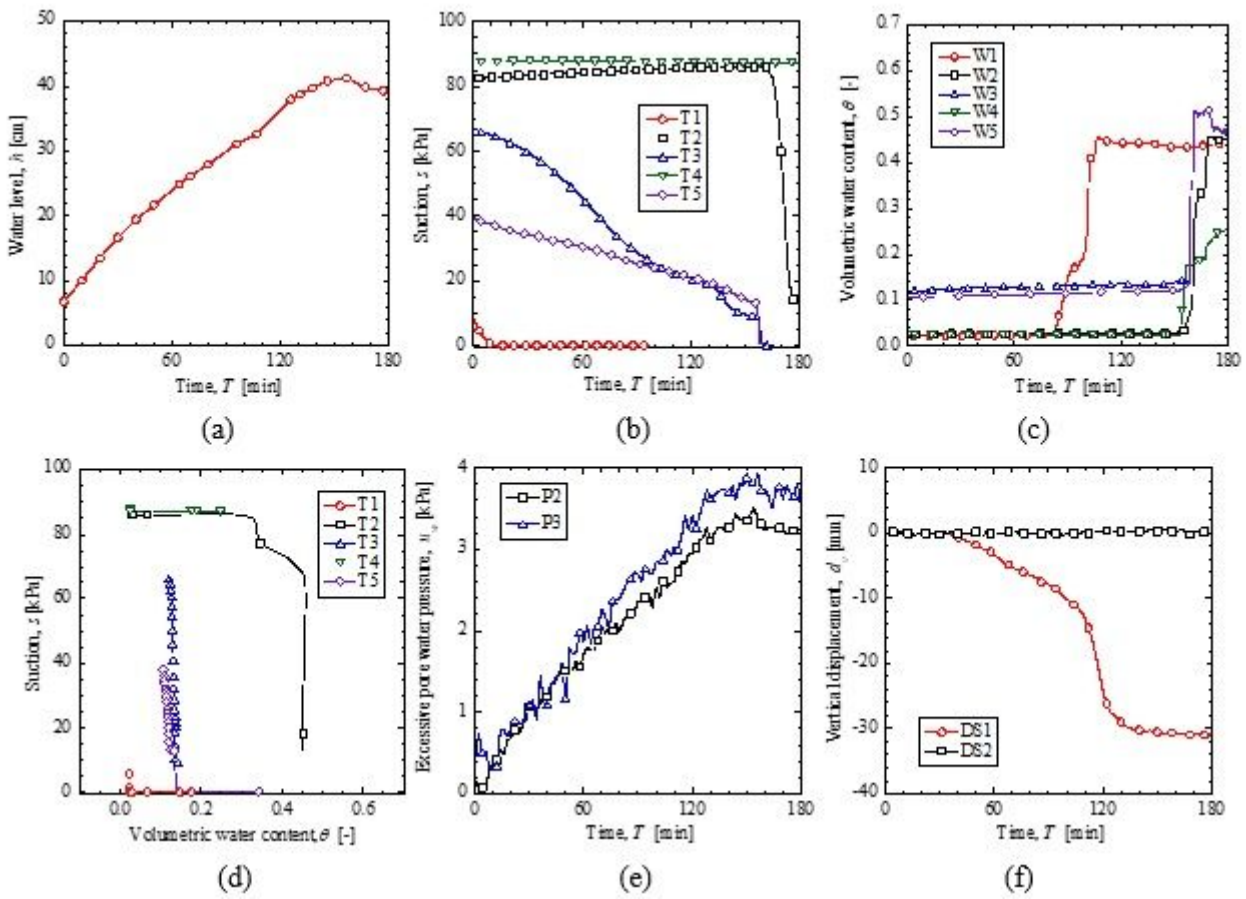
Figure 9

Time histories of the measured mechanical and physical quantities in the Case B-1 flume test
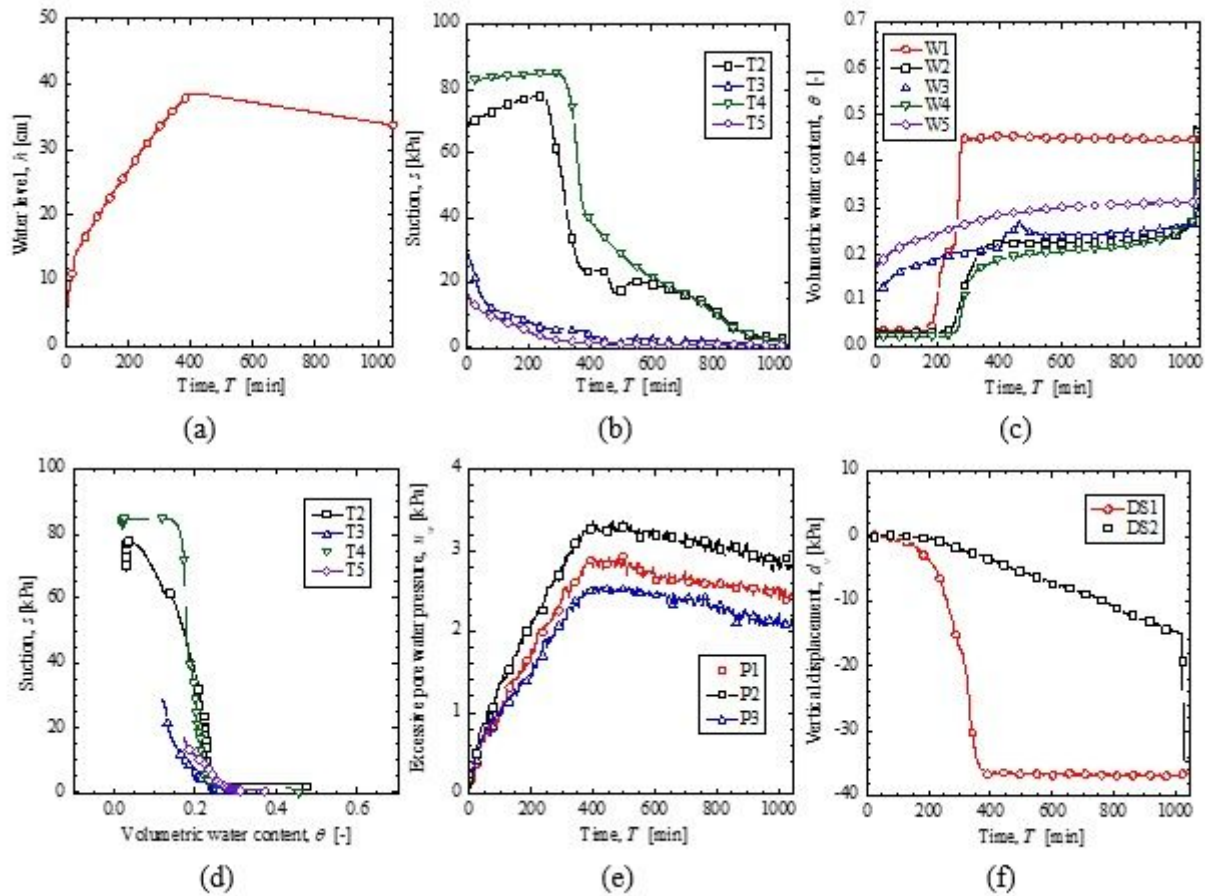
Figure 10

Time histories of the measured mechanical and physical quantities in the Case B-2 flume test
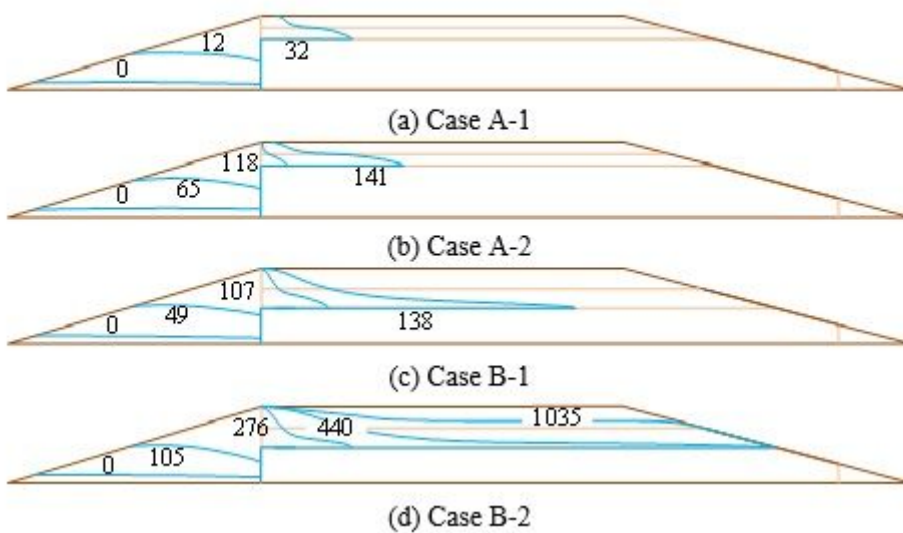
Figure 11

Development of the phreatic lines in the flume tests (unit: min)
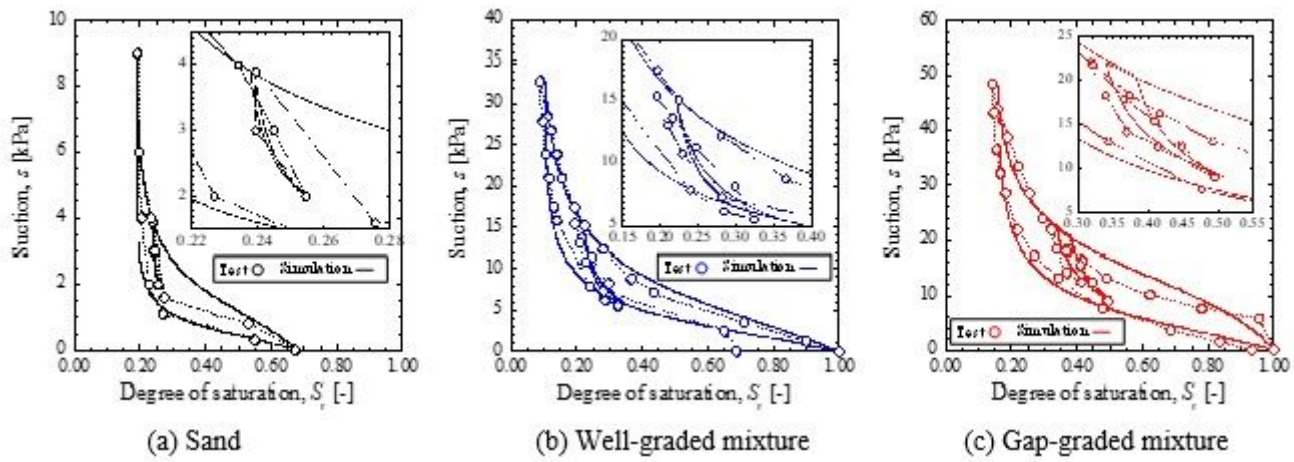
Figure 12

Water retention tests on the LD materials and corresponding element simulations

(a) Sand

(b) Well-graded mixture

(c) Gap-graded mixture
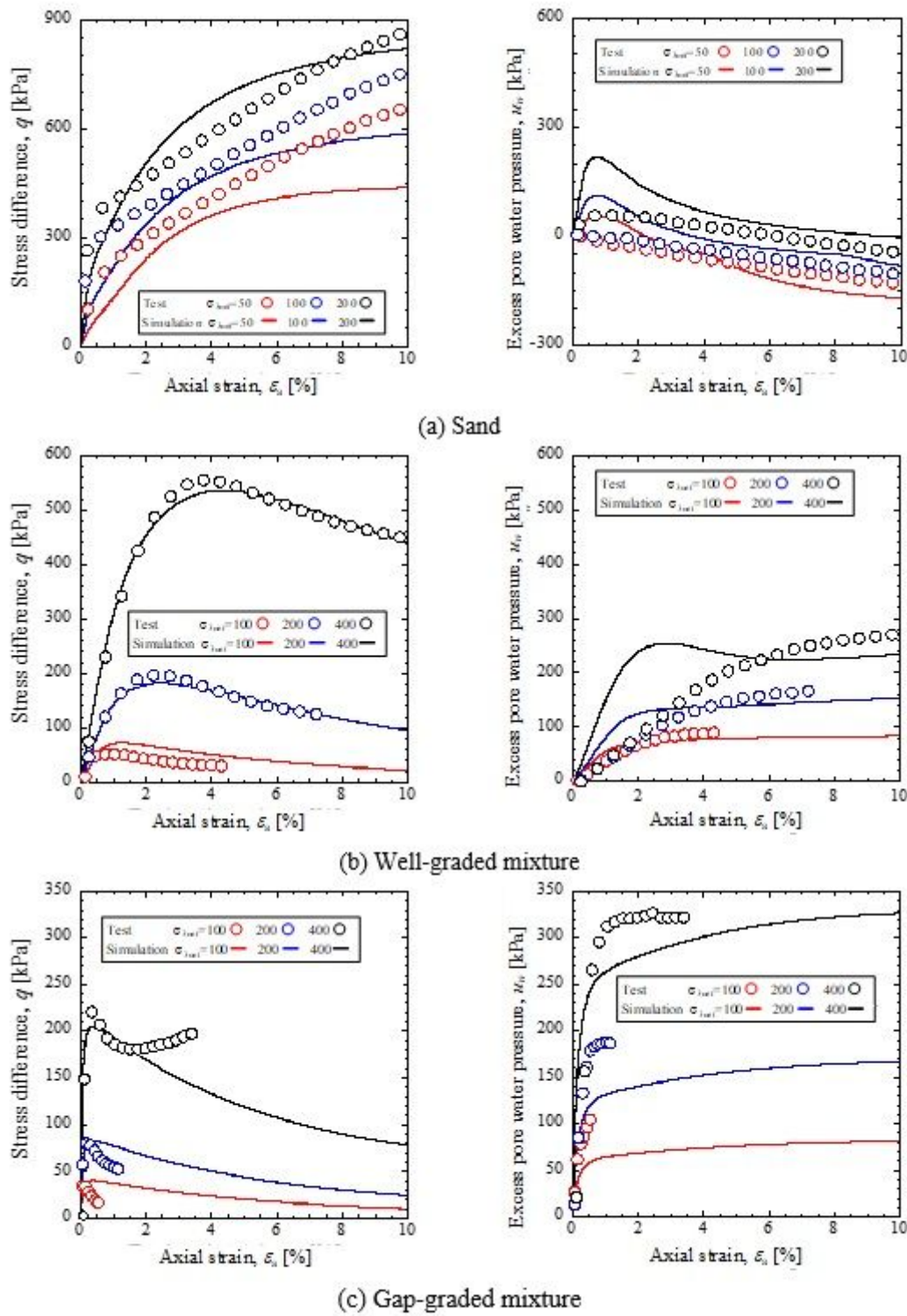
Figure 13

CU triaxial tests on the LD materials and corresponding element simulations (test data from Ma et al. (2020))
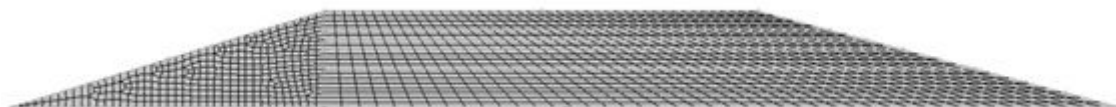
Figure 14

Finite element mesh used in the 2D FEM

1800

Drained and unvented condition

Drained and vented condition

400 mm

Undrained and unvented condition

4600 mm

(a) Hydraulic boundary condition

Free

Fixed all displacement

(b) Displacement boundary condition
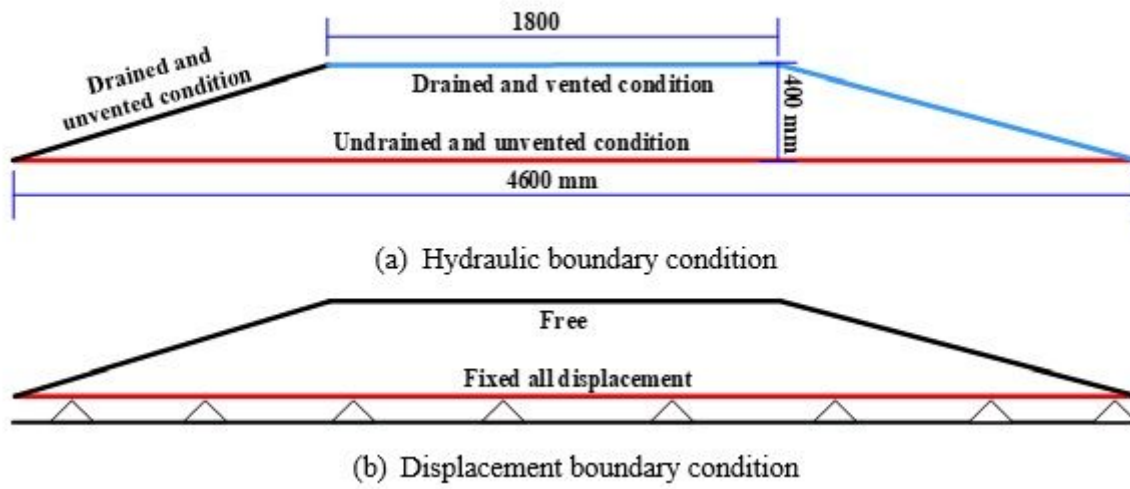
Figure 15

Mesh size and boundary conditions of the numerical model

11 13 15 17 19
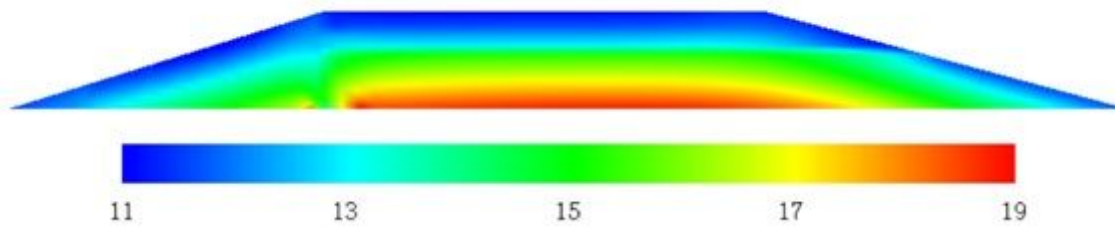
Figure 16

Initial mean effective stress field (unit: kPa)
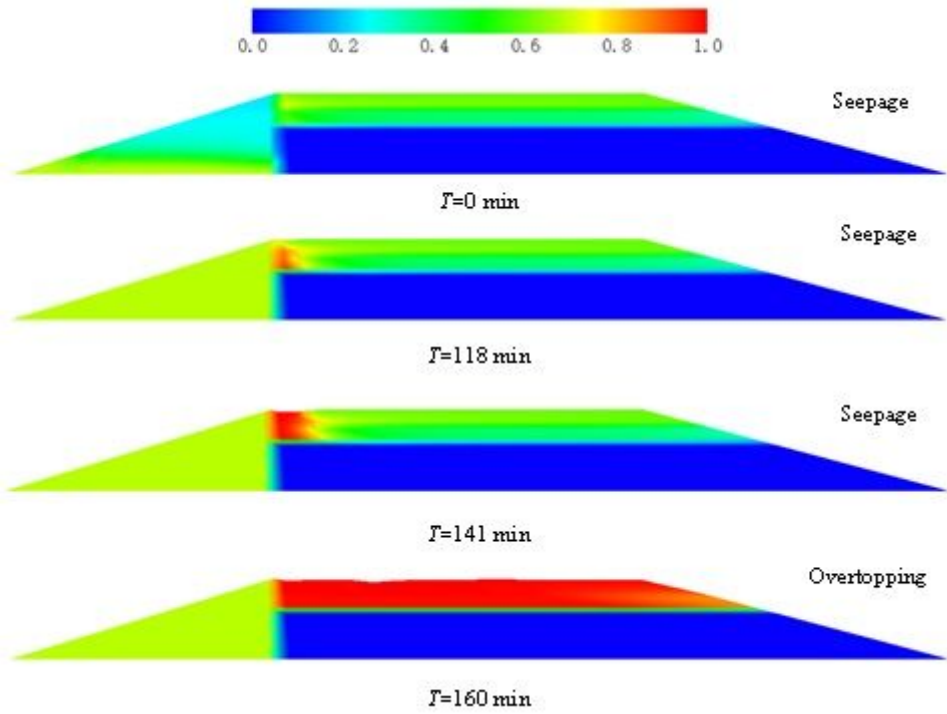
Figure 17

Calculated variation in saturation due to a rising water level for Case A-0
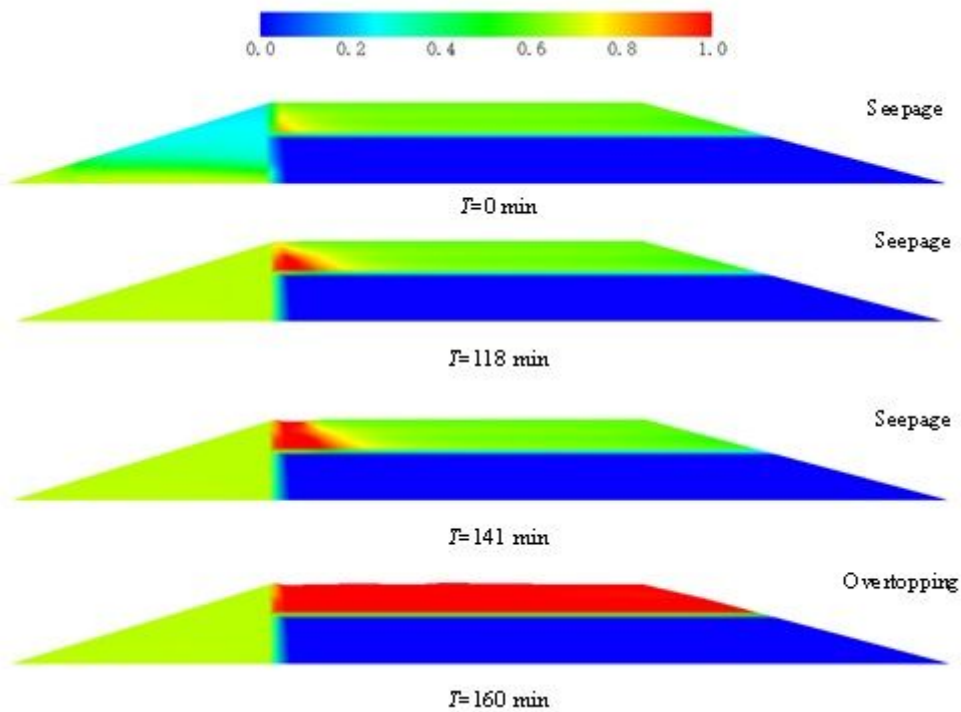
Figure 18

Calculated variation in saturation due to a rising water level in the Case A-2 flume test

(a) Change in EPWP

(b) Change in vertical displacement
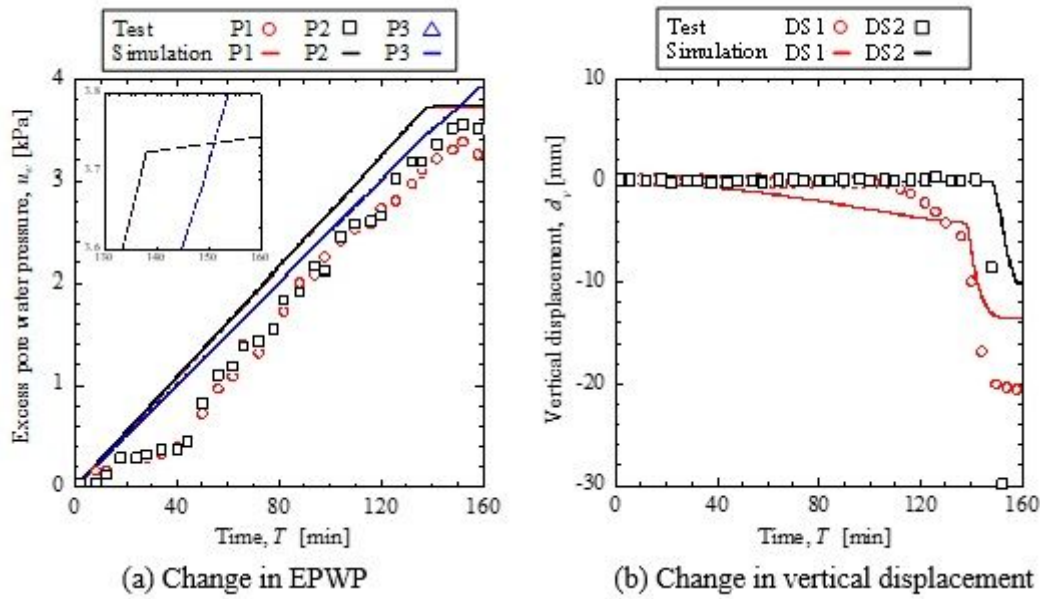
Figure 19

Test and calculated results of the mechanical quantities in the Case A-2 flume test
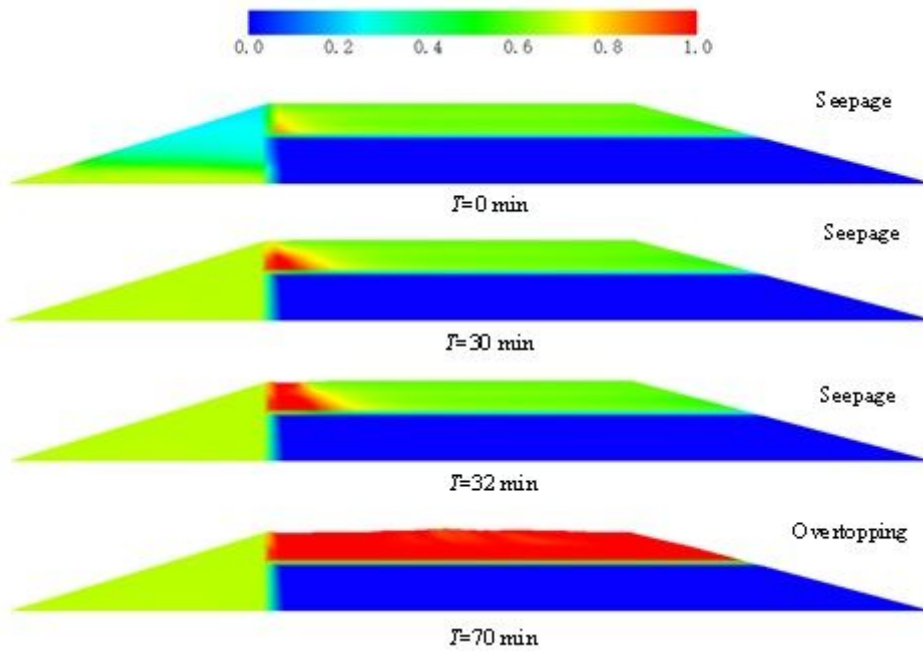
Figure 20

Simulated variation in saturation due to a rising water level in the Case A-1 flume test
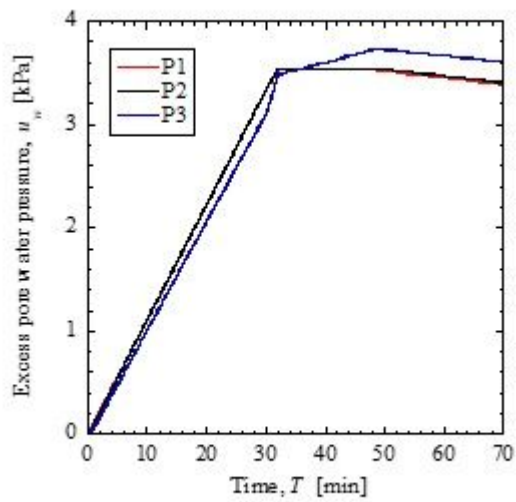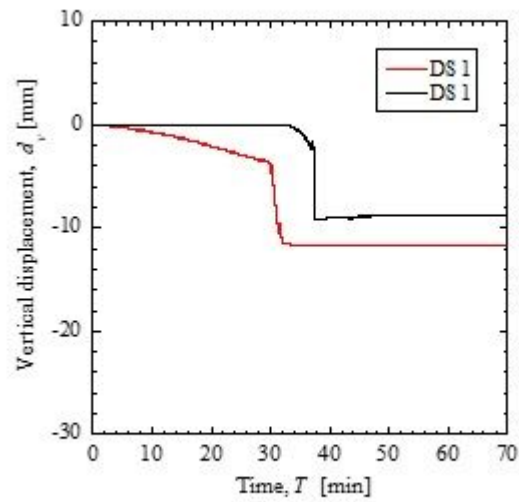
Figure 21

Simulated results for the mechanical quantities in the Case A-1 flume test
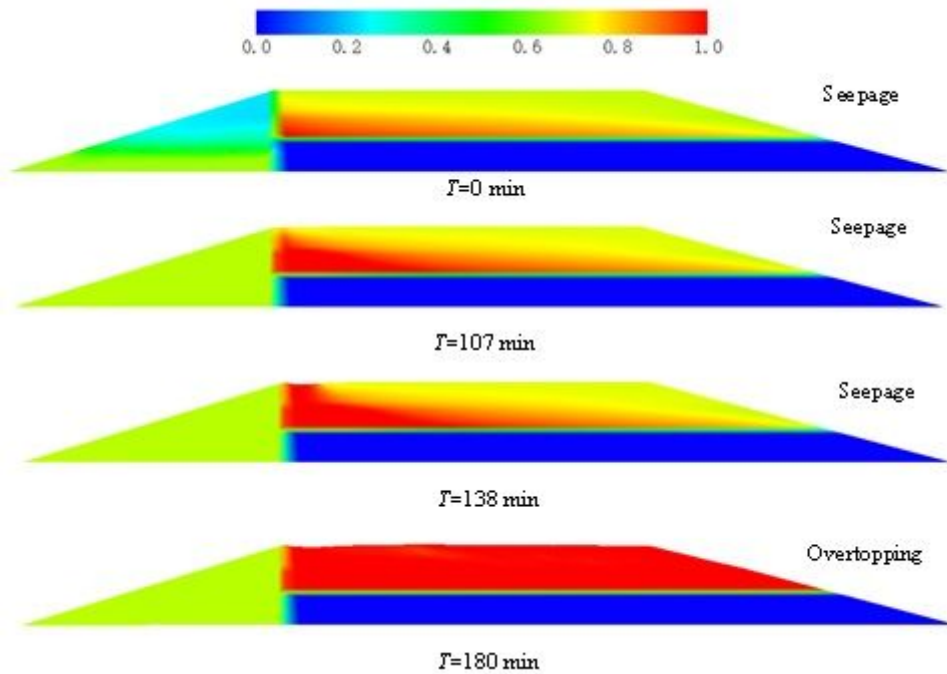
Figure 22

Simulated variation in saturation due to a rising water level in the Case B-1 flume test

(a) Change in EPWP

(b) Change in vertical displacement
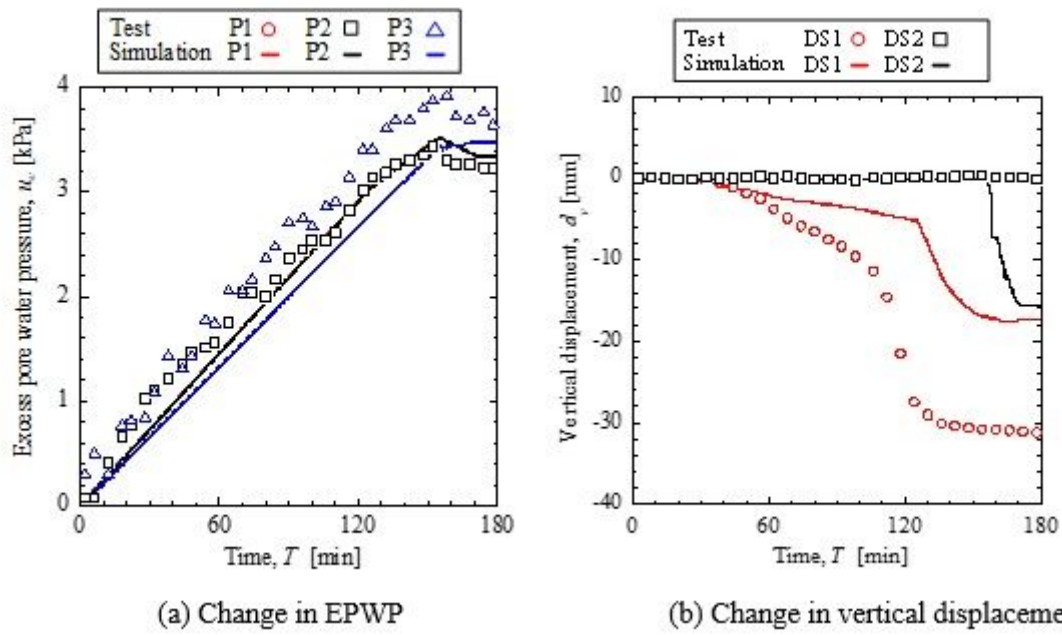
Figure 23

Test and simulated results of the mechanical quantities in the Case B-1 flume test
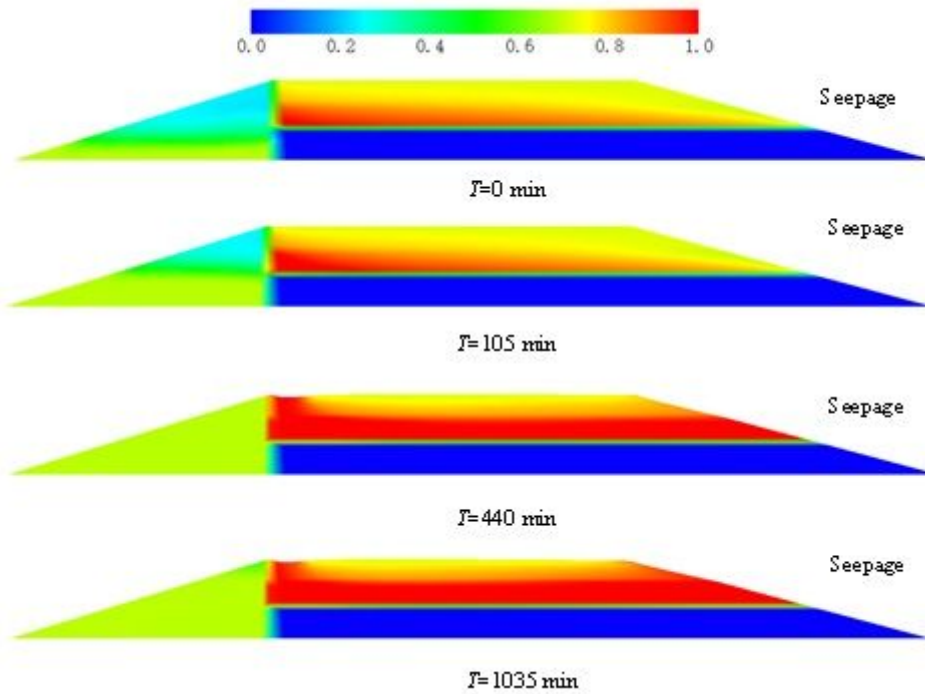
Figure 24

Simulated variation in saturation due to a rising water level in the Case B-2 flume test

(a) Change in EPWP

(b) Change in vertical displacement
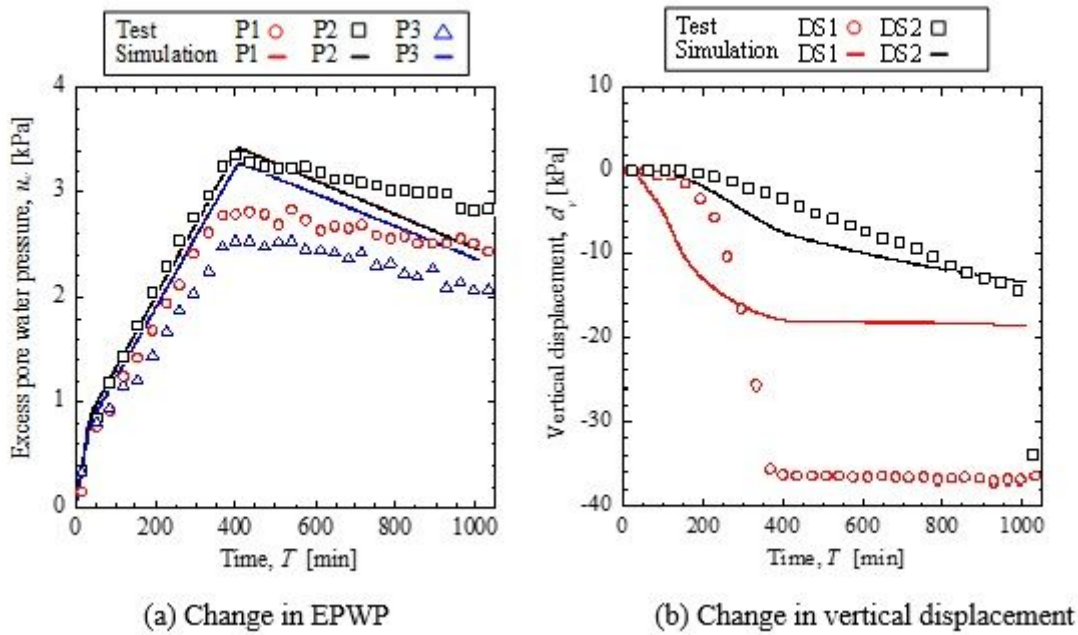
Figure 25

Test and simulated results of the mechanical quantities in the Case B-2 flume test

(a) Case A-1
$T = 70$ min

(b) Case A-2
$T = 141$ min

(c) Case B-1
$T = 138$ min

(d) Case B-2
$T = 1035$ min
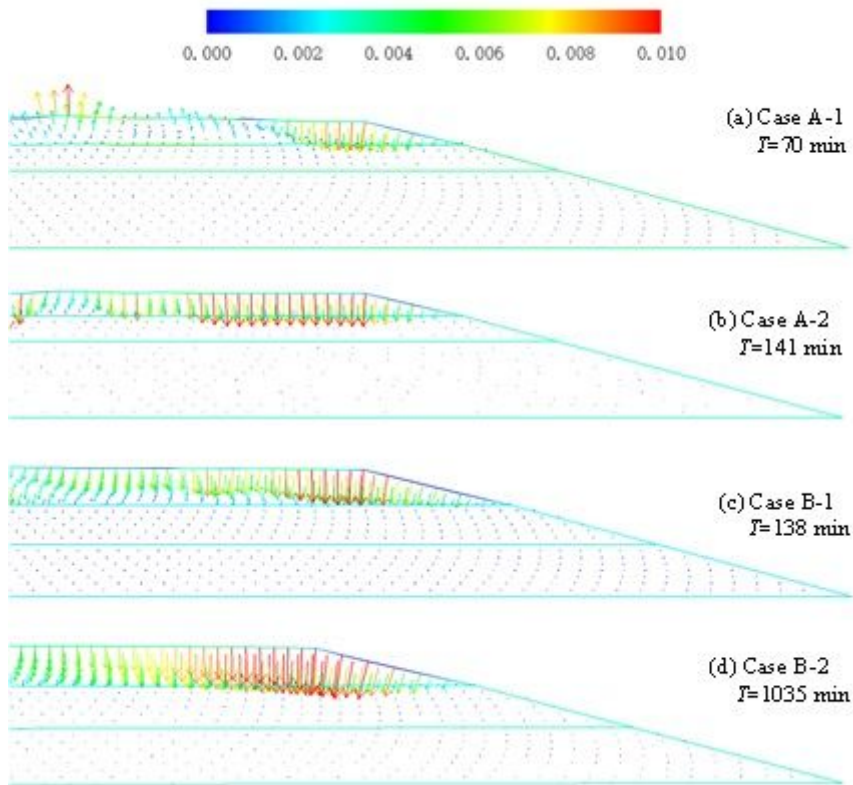
Figure 26

Distributions of the displacement vectors at the end of the flume tests (unit: m)

Supplementary Files

This is a list of supplementary files associated with this preprint. Click to download.

- Photographs.pdf